INTERNATIONAL JOURNAL FOR NUMERICAL METHODS IN FLUIDS
Int. J. Numer. Meth. Fluids 2001; **36**: 185–204

A first-order volume of fluid convection model in three-dimensional space

Seong-O. Kim*[,1], Yoonsub Sim and Eui-Kwang Kim

KALIMER Development Team, Korea Atomic Energy Research Institute, Taejon, Korea

SUMMARY

To improve the numerical analysis of free surface convections and reconstruction in a three-dimensional space, a first-order algorithm is developed based on the volume of fluid (VOF) theory. The methodology applied to the first-order method (FOM) is to define a first-order surface as near to the horizontal as possible while satisfying the defined volume fraction of a cell. The developed method is compared against the donor cell method of zeroth-order through simulation of the transitional and rotational convection of liquid spheres. Although the donor cell method shows relatively good predictions for the sphere of a large diameter, it shows poor performance of large distortions for a sphere of a relatively small diameter. However, the FOM developed in this study always shows quite satisfactory prediction results for free surface convection. Copyright © 2001 John Wiley & Sons, Ltd.

KEY WORDS: first-order method; free surface flows; three-dimensional; volume of fluid

1. INTRODUCTION

A variety of physical hydrodynamic phenomena involve interfaces between phases as shown in Figure 1(a) (where 'F' and 'V' denote a cell filled with fluid or a void respectively and 'S' denotes the surface cell partly filled with fluid and void). These interfaces can exhibit dynamic behavior and an exact mathematical description of fluid interfaces is required to solve the transport equations of motion on the fluid domain. However, the numerical description of free surface flow and interfaces is notoriously complicated due to difficulties associated with the discrete representation of the interfaces. The locations of these interfaces are not known in advance and must be determined as part of the solutions of the transport equations. There are several numerical methods for treating fluid problems with interfaces using the Lagrangian approach, such as the boundary integral technique [1–3], finite element methods [4–6] and boundary-fitted orthogonal co-ordinates [7–9]. Through these techniques, the dynamic

* Correspondence to: KALIMER Development Team, Korea Atomic Energy Research Institute, PO Box 105, Yusong, Taejon, Korea 306-600.
[1] E-mail: sokim@nanum.kaeri.re.kr

Received September 1999
Revised January 2000

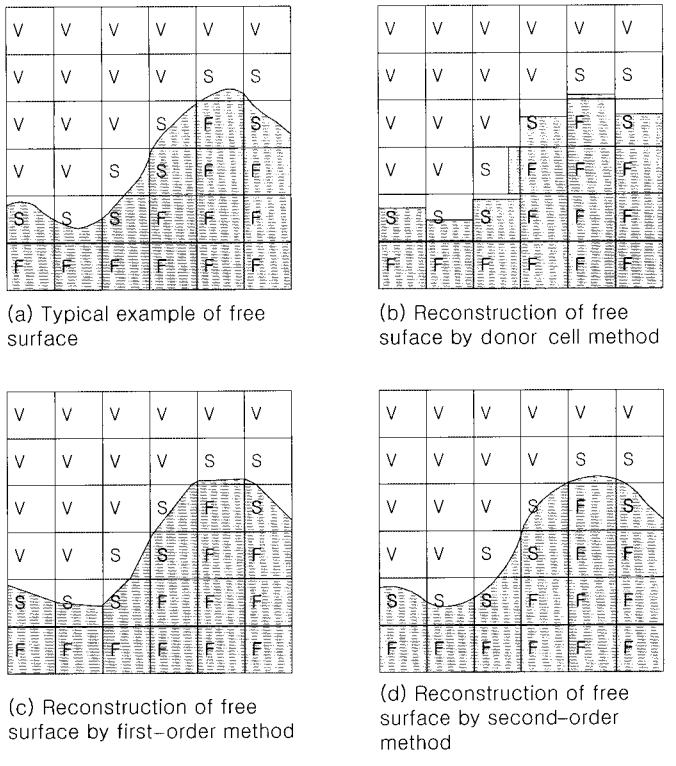

Figure 1. Typical examples and reconstruction scheme for the interfaces of free surface for two-dimensional space.

behavior of free surfaces can be calculated. However, it is difficult to handle complex phenomena, such as surface folding and surface merging, due to the discrete specification of moving points using these techniques.

A numerical technique that has the potential for handling large surface deformations, such as surface folding and merging, is the volume-tracking method. This method uses a volumetric progress variable, such as the volume of fluid (VOF) in the marker-and-cell (MAC) technique [10–12], and the VOF technique [13–16], for Lagrangian transport of the interfaces. The MAC method involves Eulerian flow field calculations and Lagrangian liquid–particle movements. The velocity of the marker is found by taking the average of the Eulerian velocities in its vicinity. One of the difficulties in using the MAC method is the possible creation of artificially high or low marker number densities in the cells due to the irregularity of the flow field. The VOF method can be applied to determine free surface curves by use of the volume fraction of a calculation cell and/or its environmental cells. This method is not susceptible to the problems that can be encountered when using the MAC method. For two-dimensional analysis, various VOF convection methods have been developed. In the earlier applications of the VOF method,

the donor cell method (DCM) of zeroth-order [17–19] was used for VOF convection calculations, where the shape in a surface cell was assumed to be either horizontal or vertical rectangular shapes as shown in Figure 1(b). To improve the accuracy of free surface convection of the DCM, Youngs [19] and Ashgriz [20] developed a first-order method (FOM) and Kim [21,22] developed a second-order method, where the interface is approximated by a first-/second-order linear equation as shown in Figure 1(c) and (d). As expected, the higher-order models show better results. Even though the higher-order methods for a two-dimensional problem improve the accuracy of free surface convection, there are difficulties when directly applying it to three-dimensional space. The reason is that, because the VOF values are discontinuous with respect to the co-ordinates at the interfaces, the VOF distribution cannot be represented by a function that is defined by a single co-ordinate variable. From these reasons, a separate technique needs to be developed for the application of the higher-order model to a three-dimensional problem. As an approach, this paper develops a first-order VOF convection model with consideration of three-dimensional effects.

2. FIRST-ORDER MODEL IN THREE-DIMENSIONAL SPACE

2.1. Concept of first-order method

The methodology for the FOM in a three-dimensional space is to find a first-order plane. If a free surface is nearly horizontal to the plane perpendicular to a z-axis and both of the VOF slopes m_x and m_y are negative, the VOF distribution function can be represented like Equation (1)

$$f = ax + by + c \tag{1}$$

The coefficients a and b of Equation (1) are obtained by equating VOF slopes with the differentiated values of the distribution function, such as Equation (2)

$$\frac{\partial f}{\partial x} = a = m_x, \qquad \frac{\partial f}{\partial y} = b = m_y \tag{2}$$

The coefficient of c in Equation (1) is obtained by equating the VOF value F to the integration of the distribution function over $\mathrm{d}x\ \mathrm{d}y$, such as Equation (3)

$$F = \iint (ax + by + c)\,\mathrm{d}x\ \mathrm{d}y \tag{3}$$

After establishing the VOF distribution function by the first-order equation, the convective fluxes of a surface cell are calculated by the integration of the equation. For the right-hand side x-face of Figure 2, the convective flux is the integration of the VOF distribution function over $\mathrm{d}x\ \mathrm{d}y$ as shown in Equation (4)

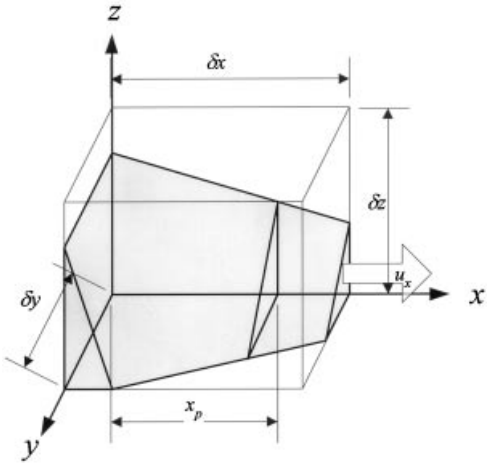

Figure 2. Free surface representation by the FOM.

$$Fxp = \int_{x_p}^{\delta x} \int_{0}^{\delta y} (ax + by + c)\, \mathrm{d}x\, \mathrm{d}y \tag{4}$$

As described above, to implement the FOM it is necessary that the slopes of the VOF distribution function need to be known and a technique needs to be developed for handling numerous cases from the slopes and the VOF value. Therefore, the FOM is implemented through the following steps in this study:

Step 1: calculation of the slopes and selection of a base plane.
Step 2: calculation of coefficients for VOF distribution function.
Step 3: calculation of convective fluxes.

2.2. Calculation of the slopes and selection of base plane

For VOF slope calculation, a cell block is used in this study so that the slope between a surface cell and a neighboring cell does not lose its accuracy even though the neighboring cell is empty. A cell block is constructed of a surface cell and its eight neighboring cells as shown Figures 3 and 4. For the x-direction slope, the VOF distribution is approximated as three cell columns that are the sum of the volume fraction from cell $(j-1)$ to cell $(j+1)$ as described by Equations (5)–(7)

$$F_{i-1} = \frac{\sum_{k=j-1}^{j+1} (\mathrm{d}y_k F_{i-1,k})}{H}, \quad H = \sum_{k=j-1}^{j+1} \mathrm{d}y_k \tag{5}$$

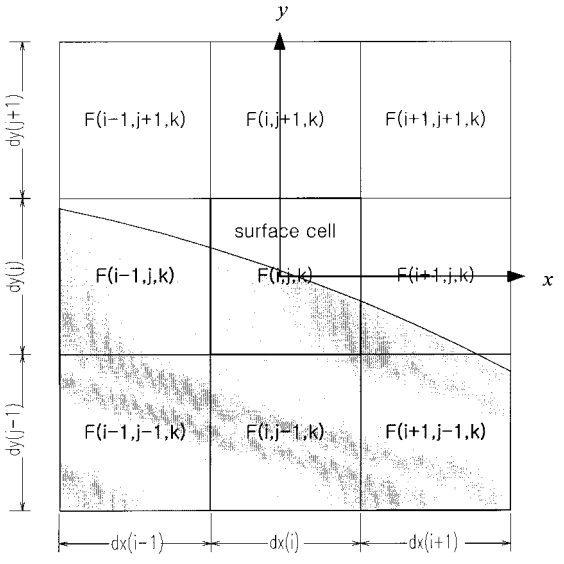

Figure 3. Cell block for x-direction slope (m_{yx}) on a y-axis plane.

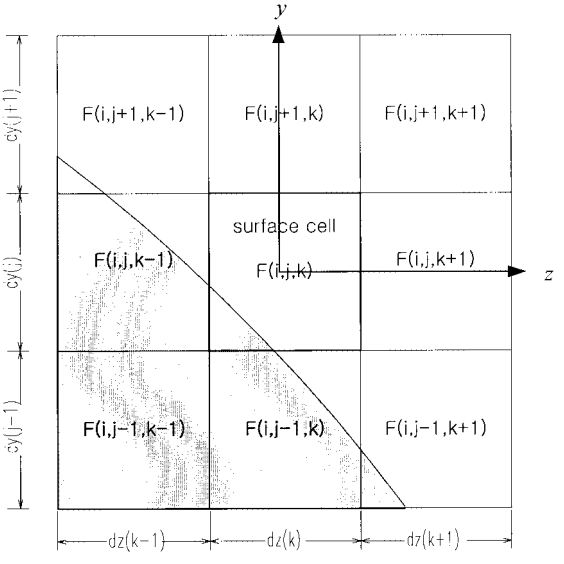

Figure 4. Cell block for z-direction slope (m_{yz}) on a y-axis plane.

$$F_i = \frac{\sum_{k=j-1}^{j+1} (\mathrm{d}y_k F_{i,k})}{H}, \quad H = \sum_{k=j-1}^{j+1} \mathrm{d}y_k \tag{6}$$

$$F_{i+1} = \frac{\sum_{k=j-1}^{j+1} (\mathrm{d}y_k F_{i+1,k})}{H}, \quad H = \sum_{k=j-1}^{j+1} \mathrm{d}y_k \tag{7}$$

The slope between the cell columns is obtained by integrating a straight line crossed over two cell columns. If the larger value of the volume fraction between the two columns is assigned as F_L and the smaller one as F_R and the cell width is represented as x_L ($= L/H$) for F_L and x_R ($= R/H$) for F_R, the slope 'm' is calculated from Equations (8)–(15) by categorizing the cases based on the value of F_L, F_R, x_L, x_R as shown in Figure 5

Case 1

$$m = -2\left[\frac{\sqrt{x_R F_R + x_L F_L} - \sqrt{x_R F_R}}{x_L}\right]^2 \tag{8}$$

if

$$F_L \geq F_R \frac{2x_R + x_L}{x_R} \quad \text{and} \quad F_L \leq 1 - \frac{[\sqrt{x_R F_R + 2x_L} - \sqrt{x_R F_R}]_2}{4x_L} \tag{9}$$

Case 2

$$m = -\frac{2(F_L - F_R)}{(x_L + x_R)} \tag{10}$$

if

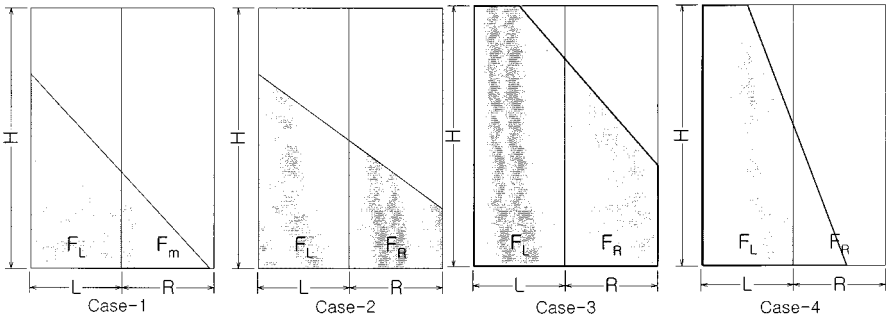

Figure 5. Calculation of slope of volume fraction between two cell columns.

$$F_L \le F_R \frac{2x_R + x_L}{x_R} \quad \text{and} \quad F_L \le \frac{x_L + x_R + x_L F_R}{2x_L + x_R} \tag{11}$$

Case 3

$$m = -2\left[\frac{\sqrt{x_R(1-F_R) + x_L(1-F_L)} - \sqrt{x_R(1-F_R)}}{x_R}\right]^2 \tag{12}$$

if

$$F_L \ge \frac{x_L + x_R + x_L F_R}{2x_L + x_R} \quad \text{and} \quad F_R \ge \frac{[\sqrt{x_L(1-F_L) + 2x_R} - \sqrt{x_L(1-F_L)}]^2}{4x_R} \tag{13}$$

Case 4

$$m = -2\left[\frac{1}{\sqrt{x_L(1-F_L)} + \sqrt{x_R(1-F_R)}}\right]^2 \tag{14}$$

if

$$F_L \le 1 - \frac{[\sqrt{x_R F_R + 2x_L} - \sqrt{x_R F_R}]^2}{4x_L} \quad \text{and} \quad F_R \le \frac{[\sqrt{x_L(1-F_L) + 2x_R} - \sqrt{x_L(1-F_L)}]^2}{4x_R} \tag{15}$$

The average slope at the center of a cell block is calculated by Equations (16)

$$\left(\frac{\mathrm{d}f}{\mathrm{d}x}\right)_{\mathrm{AVG}} = \frac{m_R \delta x_L + m_L \delta x_R}{\delta x_L + \delta x_R}, \qquad \delta x_R = \frac{\mathrm{d}x_i + \mathrm{d}x_{i+1}}{2H}, \qquad \delta x_L = \frac{\mathrm{d}x_{i-1} + \mathrm{d}x_i}{2H} \tag{16}$$

A similar calculation can be made for $\mathrm{d}f/\mathrm{d}z$ by Equations (17) and (18)

$$F_j = \frac{\sum_{k=i-1}^{i+1} \mathrm{d}x_k F_{k,j}}{H}, \quad H = \sum_{k=j-1}^{j+1} \mathrm{d}y_k \tag{17}$$

$$\left(\frac{\mathrm{d}f}{\mathrm{d}z}\right)_{\mathrm{AVG}} = \frac{m_T \delta z_B + m_B \delta z_T}{\delta z_T + \delta z_B}, \qquad \delta z_T = \frac{\mathrm{d}z_k + \mathrm{d}z_{k+1}}{2H}, \qquad \delta z_B = \frac{\mathrm{d}z_{k-1} + \mathrm{d}z_k}{2H} \tag{18}$$

In order to represent the VOF distribution by the first-order equation, a base plane needs to be established because the VOF function is defined on the base plane. The base plane is a plane perpendicular to one of the x-, y-, z-axes, where a free surface is nearly horizontal to the plane. The horizontal plane is obtained by selecting the minimum height difference ($H_{\max} - H_{\min}$) in a cell. The height difference $\mathrm{d}H$ is calculated by Equation (19) for each direction, as shown in Figure 6

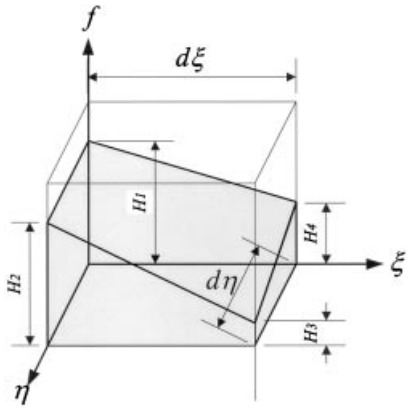

Figure 6. Representation height in a cell.

$$\mathrm{d}H = |m_\xi \, \mathrm{d}\xi| + |m_\eta \, \mathrm{d}\eta| \tag{19}$$

2.3. Calculation of coefficients for VOF distribution function

When a surface cell block is defined from the typical interface, there are a variety of free surface shapes in a surface cell. To reduce the numerous cases, the slopes of the free surface on the base plane is rearranged such that the slopes to ξ and η are negative and the absolute value of m_ξ is less than m_η. In addition, if the VOF value of the donor cell is greater than 0.5, then the definition of VOF is changed from the calculated fluid to the other fluid. By this arrangement of the slopes and VOF definition change, the basic cases are reduced to 5 as shown in Figure 7. After establishing the base cases by the method described above, the coefficients a and b are calculated by Equation (20)

$$\frac{\partial f}{\partial \xi} = a = m_\xi, \qquad \frac{\partial f}{\partial \eta} = b = m_\eta \tag{20}$$

The coefficient c of Equation (1) is calculated by equating the VOF value and the integration of the VOF distribution function. The integration of the VOF distribution function is implemented case by case. Each case is examined by comparing the value of the volume fraction F of the surface cell with the criteria as described below. If $m_\xi \neq 0$, then the cases are identified as follows:

If $F \leq Fc_{12}$, then case 1;
If $Fc_{23} \geq F \geq Fc_{12}$, then case 2;
If $Fc_{34} \geq F \geq Fc_{23}$ or $Fc_{35} \geq F \geq Fc_{23}$, then case 3;
If $F \geq Fc_{34}$, then case 4;
If $F \geq Fc_{35}$, then case 5.

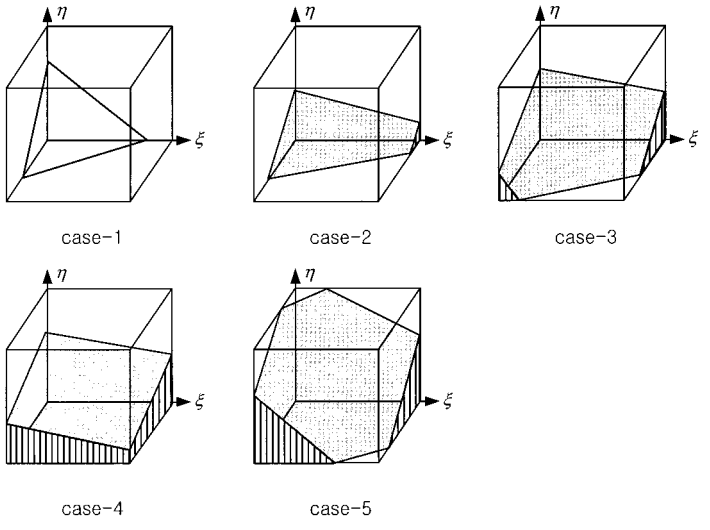

Figure 7. Possible cases for the FOM.

$$Fc_{12} = -\frac{\mathrm{d}\xi^3 m_\xi^2}{6m_\xi V} \tag{21}$$

$$Fc_{23} = -\frac{\mathrm{d}\xi(m_\xi^2\,\mathrm{d}\xi^2 - 3m_\xi\,\mathrm{d}\xi\,m_\eta\,\mathrm{d}\eta + 3m_\eta^2\,\mathrm{d}\eta^2)}{6m_\eta V} \tag{22}$$

$$Fc_{34} = -\frac{\mathrm{d}\xi\;\mathrm{d}\eta(m_\xi\,\mathrm{d}\xi + m_\eta\,\mathrm{d}\eta)}{2V} \tag{23}$$

$$Fc_{35} = -\frac{(\mathrm{d}\zeta^3 + m_\xi^3\,\mathrm{d}\xi^3 + 3m_\xi^2\,\mathrm{d}\xi^2\,\mathrm{d}\zeta + 3m_\xi\,\mathrm{d}\xi\;\mathrm{d}\zeta^2 + 3m_\eta^2\,\mathrm{d}\eta^2\,\mathrm{d}\zeta + 3m_\eta\,\mathrm{d}\eta\;\mathrm{d}\zeta^2 + m_\eta^3\,\mathrm{d}\eta^3)}{6m_\xi m_\eta V} \tag{24}$$

However, if $m_\xi = 0$, then there are only two possible cases, case 2 and case 4, and these are identified by Equation (25). If $F \geq Fc_{24}$, then case 4 and if $F \leq Fc_{24}$ then case 2. If $m_\xi = 0$ and $m_\eta = 0$, then there is only one case, case 4

$$Fc_{24} = -\frac{\mathrm{d}\xi m_\eta\,\mathrm{d}\eta^2}{2V} \tag{25}$$

2.3.1. Coefficient c calculation of the VOF distribution function. Coefficient c of Equation (1) is calculated based on the cases identified in the above section. For cases 1, 2 and 4, coefficient c is obtained explicitly and for cases 3 and 5 it is obtained by solving a third-order linear equation (29) analytically along Cardano's solution procedure [23] with the coefficients given by Equations (30) and (31) respectively.

For case 1

$$c = (6FVm_{\xi}m_{\eta})^{(1/3)} \tag{26}$$

For case 2

$$c = -\frac{m_{\xi}\,\mathrm{d}\xi}{2} + \frac{\sqrt{-3m_{\xi}^2\,\mathrm{d}\xi^2 - 72Fm_{\eta}\,\mathrm{d}\eta\,\mathrm{d}\zeta}}{6} \tag{27}$$

For case 4

$$c = F\,\mathrm{d}\zeta - \frac{m_{\xi}\,\mathrm{d}\xi + m_{\eta}\,\mathrm{d}\eta}{2} \tag{28}$$

For case 3

$$x^3 + a_1x^2 + a_2x + a_3 = 0 \tag{29}$$

$$a_1 = 3m_{\xi}\,\mathrm{d}\xi + 3m_{\eta}\,\mathrm{d}\eta$$

$$a_2 = 3m_{\xi}^2\,\mathrm{d}\xi^2 + 3m_{\eta}^2\,\mathrm{d}\eta^2$$

$$a_3 = m_{\xi}^3\,\mathrm{d}\xi^3 + 6Fm_{\xi}\,\mathrm{d}\xi m_{\eta}\,\mathrm{d}\eta\,\mathrm{d}\zeta + m_{\eta}^3\,\mathrm{d}\eta^3 \tag{30}$$

For case 5

$$a_1 = \frac{3}{2}(m_{\xi}\,\mathrm{d}\xi + m_{\eta}\,\mathrm{d}\eta - \mathrm{d}\zeta)$$

$$a_2 = \frac{3}{2}(m_{\xi}^2\,\mathrm{d}\xi^2 + m_{\eta}^2\,\mathrm{d}\eta^2 + \mathrm{d}\zeta^2)$$

$$a_3 = \frac{1}{2}m_{\xi}^3\,\mathrm{d}\xi^3 + 3Fm_{\xi}\,\mathrm{d}\xi m_{\eta}\,\mathrm{d}\eta\,\mathrm{d}\zeta + \frac{1}{2}m_{\eta}^3\,\mathrm{d}\eta^3 - \frac{1}{2}\mathrm{d}\zeta^3 \tag{31}$$

2.4. Calculation of convective fluxes

2.4.1. Rearrangement of surface cell. For calculation of convective flux, the direction of convection in the base cases must be identified since the slopes and the volume fraction of the surface cells are rearranged to reduce the number of cases. The detailed indications of ξ, η and ζ co-ordinates of the base cases relative to the real computation domain in the x-, y- and z-direction are indicated in Table I, where the z-plane is a base plane. As an example, as shown in Figure 8, shape (a) has the following properties: $|h_z| < |h_y| < |h_x|$, $m_{zx} > 0$, $m_{zy} > 0$, $F_T - F_B > 0$. The shape is rearranged based on the guide of Table I such that the ξ-, η-, ζ-axes are the reverse directions of the x, y, z co-ordinates.

Table I. Rearrangement of the FOM to reduce the base case.

Height	m_ξ	m_η	m_{zx}	m_{zy}	ξ	η	$F_T - F_B^a$	ζ	Number
$\|h_z\| < \|h_y\| < \|h_x\|$	$-\|m_{zx}\|$	$-\|m_{zy}\|$	<0	<0	$+x$	$+y$	<0	$+z$	1
			<0	<0	$+x$	$+y$	>0	$-z$	2
			<0	>0	$+x$	$-y$	<0	$+z$	3
			<0	>0	$+x$	$-y$	>0	$-z$	4
			>0	<0	$-x$	$+y$	<0	$+z$	5
			>0	<0	$-x$	$+y$	>0	$-z$	6
			>0	>0	$-x$	$-y$	<0	$+z$	7
			>0	>0	$-x$	$-y$	>0	$-z$	8
$\|h_z\| < \|h_x\| < \|h_y\|$	$-\|m_{zy}\|$	$-\|m_{zx}\|$	<0	<0	$+y$	$+x$	<0	$+z$	9
			<0	<0	$+y$	$+x$	>0	$-z$	10
			<0	>0	$-y$	$+x$	<0	$+z$	11
			<0	>0	$-y$	$+x$	>0	$-z$	12
			>0	<0	$+y$	$-x$	<0	$+z$	13
			>0	<0	$+y$	$-x$	>0	$-z$	14
			>0	>0	$-y$	$-x$	<0	$+z$	15
			>0	>0	$-y$	$-x$	>0	$-z$	16

[a] VOF difference between the top and bottom cells in the direction of the axis perpendicular to the base plane.

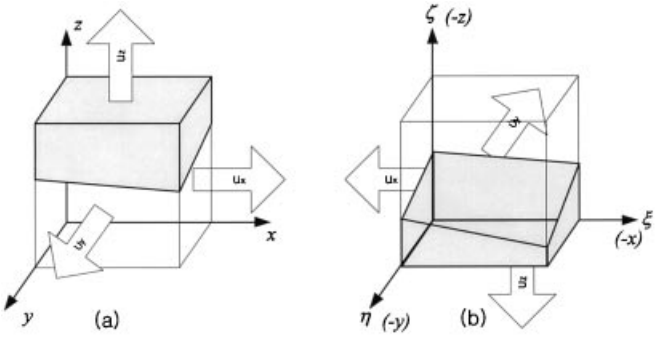

Figure 8. Rearrangement of free surface.

2.4.2. Flux calculation. After rearranging the original shape, the convective flux in the FOM is calculated via integration of the first-order equation from the cell face to the distance defined by the local velocity of the cell face over the time (Figure 9). To introduce the detailed procedure, convective flux calculations for case 1 are delineated from Equation (32)–(43) for m_ξ and m_η not zero.

Case 1

For positive ξ-direction ($\xi_p = d\xi - |u_p| \times dt$)

$$\text{if } \xi_p > \xi_1, \quad \text{then } f_{\xi_p} = 0 \tag{32}$$

$$\text{if } \xi_p < \xi_1, \quad \text{then } f_{\xi_p} = \frac{(m_\xi \xi_p + c)^3}{6 m_\xi m_\eta V} \tag{33}$$

For negative ξ-direction ($\xi_m = |u_m| \times dt$)

$$\text{if } \xi_m > \xi_1, \quad \text{then } f_{\xi_m} = F \tag{34}$$

$$\text{if } \xi_m < \xi_1, \quad \text{then } f_{\xi_m} = F - \frac{(m_\xi \xi_m + c)^3}{6 m_\xi m_\eta V} \tag{35}$$

For positive η-direction ($\eta_p = d\eta - |v_p| \times dt$)

$$\text{if } \eta_p > \eta_2, \quad \text{then } f_{\eta_p} = 0 \tag{36}$$

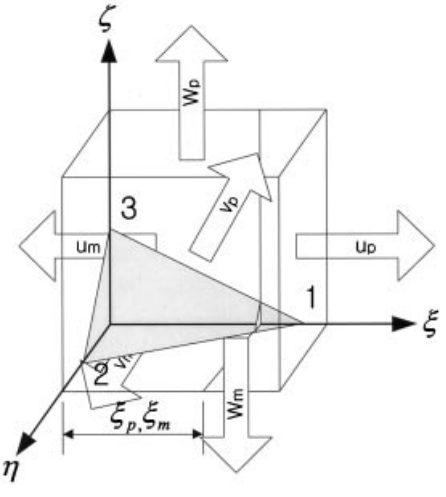

Figure 9. Convective flux calculation model.

$$\text{if } \eta_p < \eta_2, \quad \text{then } f_{\xi_p} = \frac{(m_\eta \eta_p + c)^3}{6 m_\xi m_\eta V} \tag{37}$$

For negative η-direction ($\eta_m = |v_m| \times \mathrm{d}t$)

$$\text{if } \eta_m > \eta_2, \quad \text{then } f_{\eta_m} = F \tag{38}$$

$$\text{if } \eta_m < \eta_2, \quad \text{then } f_{\eta_m} = F - \frac{(m_\eta \eta_m + c)^3}{6 m_\xi m_\eta V} \tag{39}$$

For positive ζ-direction ($\zeta_p = \mathrm{d}\zeta - |w_p| \times \mathrm{d}t$)

$$\text{if } \zeta_p > \zeta_3, \quad \text{then } f_{\zeta_p} = 0 \tag{40}$$

$$\text{if } \zeta_p < \zeta_3, \quad \text{then } f_{\zeta_p} = \frac{(c - \zeta_p)^3}{6 m_\xi m_\eta V} \tag{41}$$

For negative ζ-direction ($\zeta_m = |w_m| \times \mathrm{d}t$)

$$\text{if } \zeta_m > \zeta_3, \quad \text{then } f_{\zeta_m} = F \tag{42}$$

$$\text{if } \zeta_m < \zeta_3, \quad \text{then } f_{\zeta_m} = F - \frac{(c - \zeta_m)^3}{6 m_\xi m_\eta V} \tag{43}$$

For the other cases the convective flux is calculated in the same way.

3. RESULTS AND DISCUSSION

3.1. Reconstruction of free surface

To assess the capability for reconstruction of free surfaces, a spherical liquid drop is reconstructed by the present method, as shown Figure 10, based on the VOF calculated by an analytical method. The outermost circle represents the interface at the center of the liquid drop to the z-direction. The concentric circles are interfaces of the sections at the radius of 3–4 times that of a cell size to the z-axis direction with an increment of 0.2 times the cell size. However, the liquid drop is reconstructed as square boxes by the DCM of Hirt and Nichols, since the VOF is assumed to be constant within a cell, as shown in Figure 11.

3.2. Transitional convection of a sphere

The FOM developed in this study is tested and compared with the DCM for the convection of liquid spheres. The DCM used in this study is from Martin [24] for three-dimensional free surface convection. A uniform velocity field is assigned for the entire calculation region to the positive x-, y-, z-directions. The velocities in the field are assigned as one quarter of a cell size,

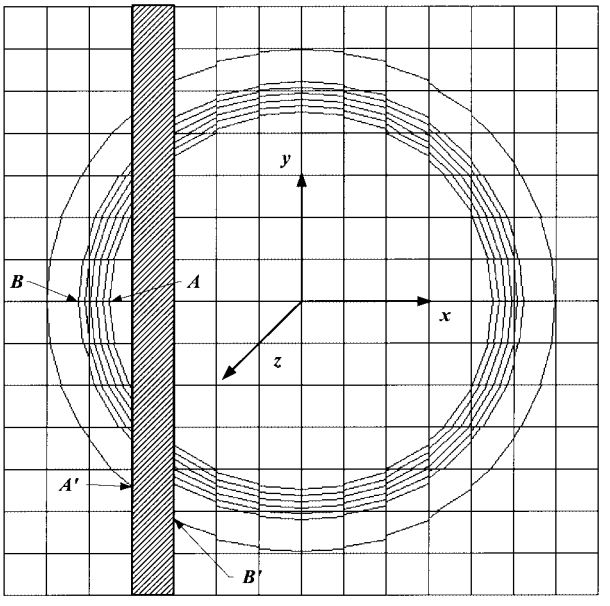

Figure 10. Reconstruction of liquid sphere with radius 6.0–7.0 times the mesh cell.

which is of uniform length in this study in every direction. The sphere is convected with this velocity for 80 time steps until the largest sphere completely moves out of its original location. The calculation results are reviewed against three types of numerical errors. The first one is a maximum cell convection error, which can be an indication of local shape deformation. The second is the square-root-of-the-square-sum (SQRSS) of every cell error for an indication of overall convection error. The final one is a total volume change to measure the conservation of volume fraction during total convection period. The convection error of a cell is defined as the cell volume fraction difference between original analytical input data and the value of the VOF after the convection to the final time step for each cell, and those are normalized to the total volume of each sphere.

The normalized maximum cell errors for each convection method are shown in Figure 12 for transitional convection. The DCM and the FOM show a continuous decrease with increasing numbers of cells for the radius of the sphere. The error of the FOM is one-third or one-quarter of the DCMs for small-radius spheres but is over one tenth of the DCMs for large-radius spheres. It is representative that the FOM has much less local distortions from the original shape than the DCM. Comparing the slopes of error in the semi-log plots, the maximum error of the FOM is decreasing more rapidly than that of the DCM. It may be reasoned that as the number of cells increases, the free surface of a circle can be represented exactly by the segments of the first-order curve as the circle diameter increases. The SQRSS errors for both methods are shown in Figure 13, where the error has a similar tendency to the maximum cell error. The magnitude of the SQRSS error of the FOM is almost one-tenth of that of the DCM. The

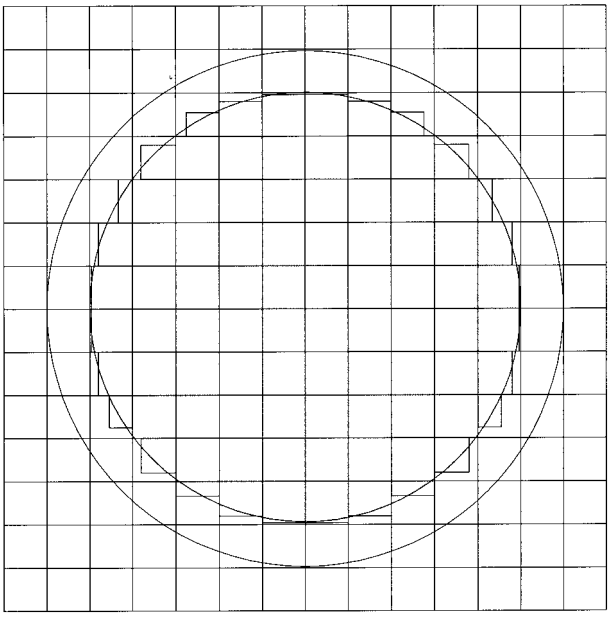

Figure 11. Reconstruction of liquid sphere with radius 6.0–7.0 times the mesh cell.

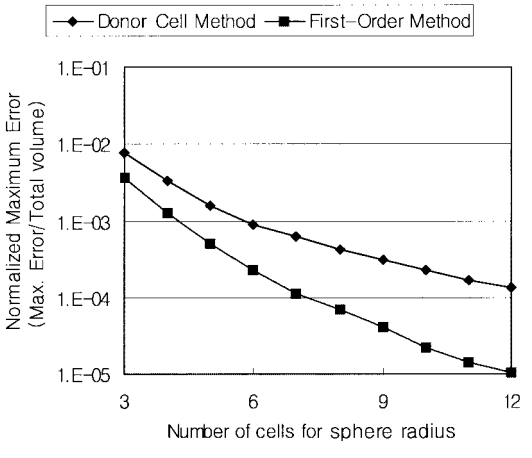

Figure 12. Maximum cell error vs sphere radius after 80 time step transitional convections.

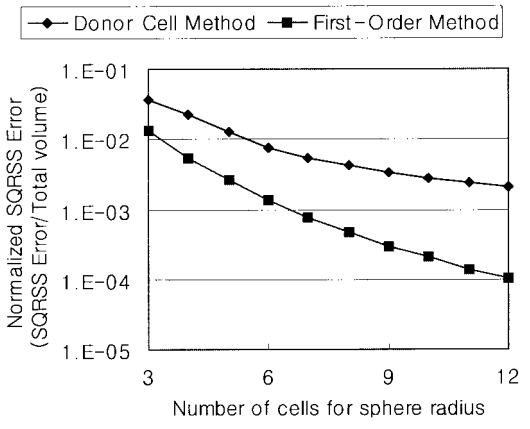

Figure 13. SRSSE vs sphere radius after 80 time step transitional convections.

SQRSS error of the FOM decreases more rapidly than the one of the DCM as the number of cells increases. This feature may be due to the same reasons as that of the one described for the maximum error. The magnitude of the SQRSS means a deviation of convection errors in each cell. As the SQRSS increases, the probability for deviation of the convected VOF value from the analytical data increases and vice versa. The volume changes by VOF convection are examined since they may impact the continuity equation for pressure calculation in solving the momentum equations of incompressible flow. The normalized volume changes for each method are shown in Figure 14. The amount of the volume change with respect to the radius for FOM varies around 1.0×10^{-6} and the value for DCM varies around 3.0×10^{-5}. From the above results, the total volume change of the FOM is slightly less than the one of the DCM but is almost the same for both free surface convection methods. To visualize the convection results, three views of the reconstructed sphere are shown in Figure 15. The leftmost one is for an original sphere with a radius of eight cells and the center one is for the sphere after an 80-time step convection by the FOM and the rightmost one is for the sphere after the DCM. As shown in Figure 15, the reconstructed shape of the FOM convection maintains almost its original shape. However, the reconstructed shape after convected by the DCM was badly distorted. This is consistent with the results of Figures 12 and 13. From the results it is known that the FOM has a better capability than the DCM in transitional convection of spherical shapes.

3.3. Rotational convection of a sphere

To compare the performance of each method for a rotational flow, various sizes of liquid sphere are examined for a uniform angular velocity. The angular velocity is assumed such that the maximum circumferential velocity of the maximum size of liquid sphere is one quarter of a uniform cell size. The sphere is turned on an axis (z-axis) with the velocity until it rotates around completely. After convection, the normalized maximum error between the two methods is compared, as shown in Figure 16. The magnitude of the maximum error of the FOM varies

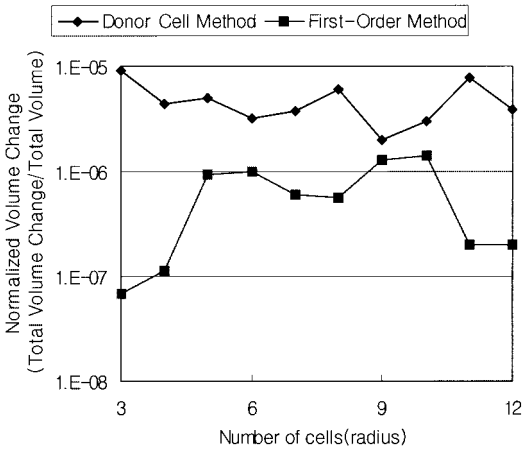

Figure 14. Volume change of FOM and DCM after 80 time step transitional convections.

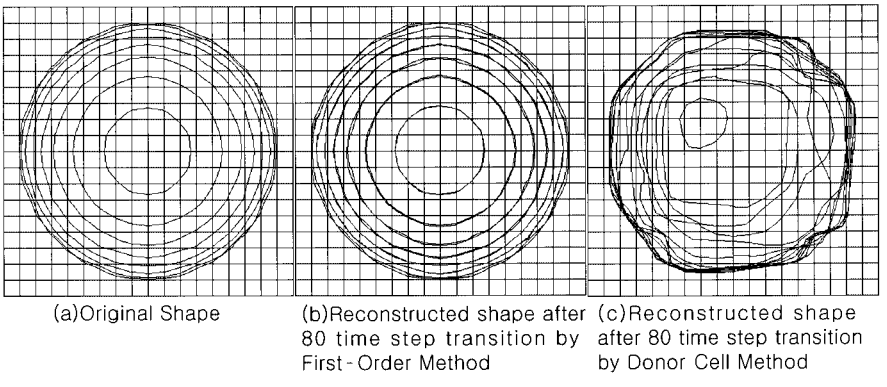

Figure 15. Reconstruction of a spherical liquid drop after 80 time step transitional convection by the FOM and DCM.

from one-tenth to one-fiftieth of that of the DCM. The SQRSS error and the volume change for both of the methods are shown in Figures 17 and 18, where both errors have similar tendency to the transitional convection. To visualize the accuracy of the convection, three views of the reconstructed sphere are shown in Figure 19. The leftmost one is a drawing for an original sphere with a radius of eight cells, the center one is for the sphere after a 300-time step convection by the FOM and the rightmost one is for the sphere after the DCM. As shown in the figure, the reconstructed sphere of the FOM convection almost maintains its original shape. However, the reconstructed sphere after convection by the DCM is badly distorted. This is consistent with the results of Figures 16 and 17. From the results, it is known that the FOM has a much better capability than the DCM for rotational convection of the sphere also.

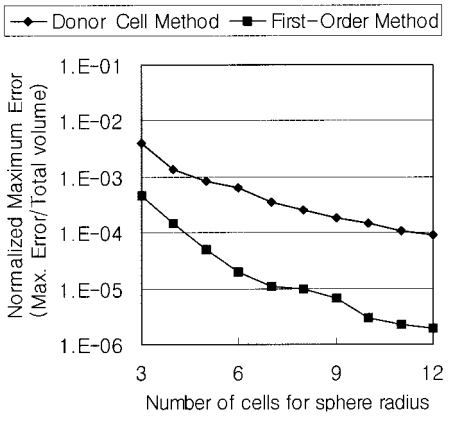

Figure 16. Maximum cell error vs sphere radius after 300-time step rotational convections.

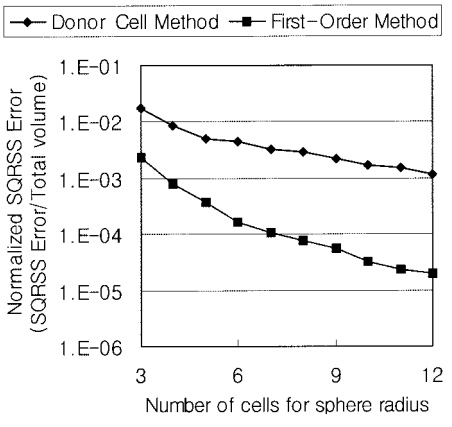

Figure 17. SRSSE vs sphere radius after 300 time step rotational convections.

4. CONCLUSIONS

A new technique for the interface transport and reconstruction of the free surface in a three-dimensional space was developed for the numerical models of the volume fraction method. The basic features of this technique are to represent the free surface and to calculate the convective flux by utilization of a set of first-order equations. This technique was tested for the various sizes of spheres for transitional and rotational convection. For both of the tests, the reconstructed shape of the sphere after convection by the DCM shows an extremely distorted one. On the other hand, the reconstructed shape of the sphere after the convection by the FOM almost shows the original shape. From the test, it was found that the total volume

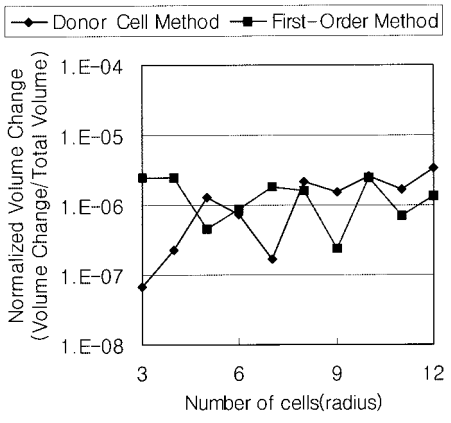

Figure 18. Total volume change vs sphere radius after 300 time step rotational convections.

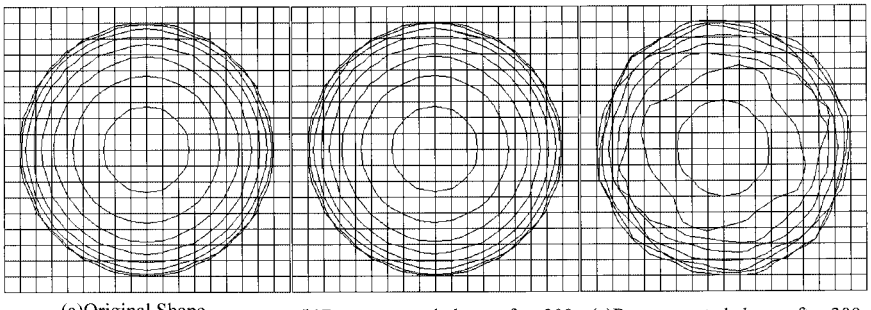

Figure 19. Reconstruction of a spherical liquid drop after 300 time step rotational convection with uniform angular velocity.

change is negligibly small for all the free surface convection models tested, but the maximum error and the SQRSS error of a cell heavily depend on the convection model tested and the errors are good indicators of the accuracy of the convection model explicitly. In conclusion, it is known that the FOM is recommended to achieve better accuracy for the reconstruction and convection of free surface in a three dimensional space.

ACKNOWLEDGMENTS

This work was performed under the Long-and-Mid-term Nuclear R&D Program sponsored by the Ministry of Science and Technology of Korea.

REFERENCES

1. Milthorpe JF, Tanner RI. 'Boundary element method for free surface viscous flows', Proc. 7th Australasian Conf. on Hydraulics & Fluid Mechanics, Preprints of Papers (Brisbane, Australia: 18–22 August, 1980), Barton, Australia, Inst. Engrs. Aust., 1980, pp. 103–106. (Nat. Conf. Publication No. 80/4), 1980.
2. Makoto N, Kawarada H. Numerical solution of free surface drainage problem of twoimmiscible fluids by the boundary element method. *Japanese Journal of Applied Physics* 1985; **24**(10): 1359–1362.
3. Henderson HC, Kok M, De Koning WL. Computer-aided spillway design using the boundary element method and non-linear programming. *International Journal for Numerical Methods in Fluids* 1991; **13**: 625–641.
4. Bonnerot R, Jamet P. Numerical computation of the free boundary for the problem by space-time elements. *Journal of Computational Physics* 1977; **25**: 163–181.
5. Lynch DR. Unified approach to simulation on deforming elements with application to phase change problems. *Journal of Computational Physics* 1982; **47**: 387–411.
6. Bach P, Hassager O. An algorithm for the use of the Lagrangian specification in Newtonian fluid mechanics and applications to free-surface flow. *Journal of Fluid Mechanics* 1985; **152**: 173–190.
7. Kang IS, Leal LG. Numerical solution of axisymmetric, unsteady free-boundary problems at finite Reynolds number. I. Finite-difference scheme and its application to the deformation of a bubble in a uniaxial straining flow. *Physics of Fluids* 1987; **30**(7): 1929–1940.
8. Ryskin G, Leal LG. Numerical solution of free-boundary problems in fluid mechanics. Part 1. The finite-difference technique. *Journal of Fluid Mechanics* 1984; **148**: 1–17.
9. Asaithambi NS. Computation of free-surface flows. *Journal of Computational Physics* 1987; **73**: 380–394.
10. Harlow FH, Welch JF. Numerical calculations of time-dependent viscous incompressible flow of fluid with free surface. *Physics of Fluids* 1965; **8**: 2182–2189.
11. Chan RK-C, Street RL. A computer study of finite-amplitude water waves. *Journal of Computational Physics* 1970; **6**: 68–94.
12. Miyata H. Finite difference simulation of breaking waves. *Journal of Computational Physics* 1986; **65**: 179–214.
13. Hirt CW, Nichols BD. Volume of fluid (VOF) methods for the dynamics of free boundaries. *Journal of Computational Physics* 1981; **39**: 201–225.
14. Nichols BD, Hirt CW, Hotchkiss RS. SOLA-VOF: a solution algorithm for transient fluid flow with multiple free boundaries. Los Alamos Scientific Laboratory Report No. La-8355, 1980.
15. Partom IS. Application of the VOF method to the sloshing of a fluid in a partially filled cylindrical container. *International Journal for Numerical Methods in Fluids* 1987; **7**: 535–550.
16. Noh WF, Woodward P. SLIC (Simple Line Interface Calculation), *Proceedings of the 5th International Conference on Numerical Methods in Fluid Dynamics*, *Lecture Notes in Physics*, Vol. 59, van de Vooren AI, Zandbergen PJ (eds). Springer: New York, 1976.
17. Chorin AJ. Flame advection and propagation algorithm. *Journal of Computational Physics* 1980; **35**: 1–11.
18. Chorin AJ. Curvature and solidification. *Journal of Computational Physics* 1985; **57**: 472–490.
19. Youngs DL. In *Numerical Methods for Fluid Dynamics*, Morton KW, Baines MJ (eds). Academic Press: New York, 1982.
20. Ashgriz N, Poo JY. FLAIR (flux line-segment model for advection and interface reconstruction). *Journal of Computational Physics* 1991; **93**: 449–468.
21. Kim S-O, No HC. Second-order model for free surface convection and interface reconstruction. *International Journal for Numerical Methods in Fluids* 1998; **26**: 79–100.
22. Kim S-O, Cho B-H. Second-order convection model in non-orthogonal coordinates. *Computational Fluid Dynamics Journal* 1998; **6**(4): 427–437.
23. Spiegel MR. *Mathematical Handbook of Formulas and Tables in Schaum's Outline Series*. McGraw-Hill, 1968.
24. Torrey MD. NASA-VOF3D: a three dimensional computor program for incompressible flows with free surface. LA-11009-MS, July, 1987.

